Inorganic Chemistry Communications 166 (2024) 112671

Contents lists available at ScienceDirect

Inorganic Chemistry Communications

journal homepage: www.elsevier.com/locate/inoche

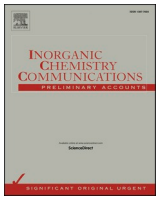

Short communication

Wastewater treatment via H_2O_2 activation and 4-nitrophenol oxidation with iron-doped nickel-azolate frameworks

Nuria Martín [a,*,1], Elena López-Maya [b,1], Miguel Maireles-Porcar [a], Mayra G. Álvarez [b], Jordi Llorca [c], Belén Altava [a], Eduardo García-Verdugo [a], Francisco G. Cirujano [a,*]

[a] Department of Inorganic and Organic Chemistry, Universitat Jaume I., Av. Sos Baynat, s/n, 12006 Castelló de la Plana, Spain
[b] Department of Inorganic Chemistry, University of Salamanca, GIR-QUESCAT Group, Pl. Caídos, s/n, 37008 Salamanca, Spain
[c] Department of Chemical Engineering and Barcelona Research Center in Multiscale Science and Engineering, Eduard Maristany 10–14, 08019 Barcelona, Spain

ARTICLE INFO

Keywords:
Fenton
MOFs
Iron
H_2O_2
Nitrophenol
Oxidation
Catalyst

ABSTRACT

An advanced oxidation heterogeneous process completely degrades 4-nitrophenol in weak acid ambient aqueous conditions using post-synthetically iron-doped nickel azolate frameworks. The framework crystallinity, porosity and reactivity of the redox-active iron (II/III) sites, hydroxyl anions and radicals upon H_2O_2 pretreatment are discussed based on spectroscopic analysis of the reaction mixture and pretreated MOF.

1. Introduction

Anthropogenic activity leads to the presence of organic pollutants in water, such as nitrophenols, which are toxic and limit the number of potable water due to their notable presence in the water reservoir [1]. Indeed, nitroaromatics such as the common p-nitrophenol pollutant, exhibit significant solubility in water and thus important environmental impact [2]. Therefore multiple methods are proposed for its elimination such as distillation, adsorption, biodegradation, chemical oxidation, electrochemical oxidation, enzymatic treatment, and membrane technology [3]. Among them, catalytic/chemical oxidation methods such as the Fenton reaction, where Fe^{2+} catalyzes the decomposition of H_2O_2 to produce hydroxyl radicals ($^{\bullet}OH$) are the most effective and relatively cheap [4]. However, the low cycle efficiency of Fe(II)/Fe(III), the narrow pH range, and the generation of iron sludge are among the most common drawbacks. In Scheme 1 we summarize, on the one hand, the reduction of Fe(III) to Fe(II) by H_2O_2, resulting in protons and reactive oxygen species (ROS), such as $HO_2^{\bullet}$ and $O_2^{\bullet}$. On the other hand, the Fe(II) sites can split hydrogen peroxide into the desired OH· radicals, which are highly reactive in the Fenton oxidation of organics (into CO_2 and H_2O for the total oxidation/degradation).

The design of bioinspired iron-containing peroxidase-like chemo catalysts is highly desired [5], given the efficiency of hemo-based enzymes in the degradation of phenyl-containing contaminants into less toxic intermediates, such as small acids, CO_2 and H_2O [6]. However, the narrow range of temperature, pH, and organics that biocatalysts can withstand before deactivating, encourages the development of robust heterogeneous catalysts. To stabilize the active site, as well as to facilitate the recycling and recovery of the iron sites, heterogeneous catalysts have been proposed for the Fenton reaction [7]. On the one hand, zeolites with iron sites were active in the removal of phenol at relatively mild temperatures of 70 °C and an acidic pH [8]. On the other hand, metal–organic frameworks (MOFs) have recently gained attention as heterogeneous catalysts due to the high dispersion and isolation of the metal sites, e.g. Fe(III)/(II), and the optimal hydrophilicity and dispersibility of the heterogeneous catalyst in water solutions [9,10].

This fact allows its application as heterogeneous catalysts to generate considerable density of ($^{\bullet}OH$) active sites able to interact with the organic pollutant of the water, promoting their degradation [11]. Terephthalic (1,4-benzene dicarboxylic acid) and/or trimesic (1,3,5-benzene tricarboxylic acid) carboxylate-based MOFs, such as MIL-53, MIL-88B, MIL-100, MIL-101, are almost exclusively employed. In this case, relatively bulky phenol-like substrates and peroxide oxidant species reach the active sites situated at both external and internal active sites

* Corresponding authors.
E-mail addresses: numartin@uji.es (N. Martín), cirujano@uji.es (F.G. Cirujano).
[1] These authors contributed equally.

https://doi.org/10.1016/j.inoche.2024.112671
Received 28 April 2024; Received in revised form 30 May 2024; Accepted 31 May 2024
Available online 1 June 2024

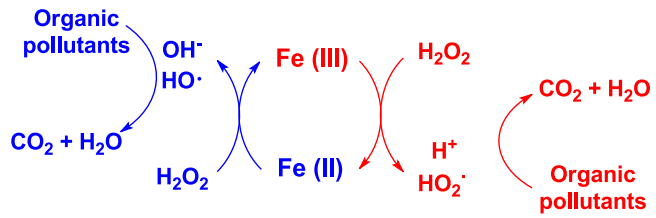

Scheme 1. H_2O_2 decomposition into protons and superoxide ions (at the Fe (III), red at the top right part), or hydroxyl radicals and anions (at the Fe(II), blue at the bottom left part).

within the MOF porous crystalline nanoparticles. Although relevant catalytic performance has been demonstrated for these systems under mild oxidation conditions (e.g. complete oxidation at room temperature pH = 4 and 30 min of reaction) [12], there may be some drawbacks that could limit their practical application in the environmental remediation of wastewater. On the one hand, the weakness of Fe(II/III)-carboxylate bonds compromises the MOF structure (with respect to robust chromium terephthalates), often resulting in iron dissolution and/or the formation of iron oxide MOF-derived species [13]. On the other hand, using stoichiometric amounts of metal results in a large proportion of those sites (located at inner parts of the crystal) not available to reaction substrates. Thus, new design approaches of MOF nanomaterials containing catalytic amounts of isolated iron sites grafted to the linkers through strong coordination bonds are needed.

Herein we take advantage of the well-isolated Fe(III/II) sites in a

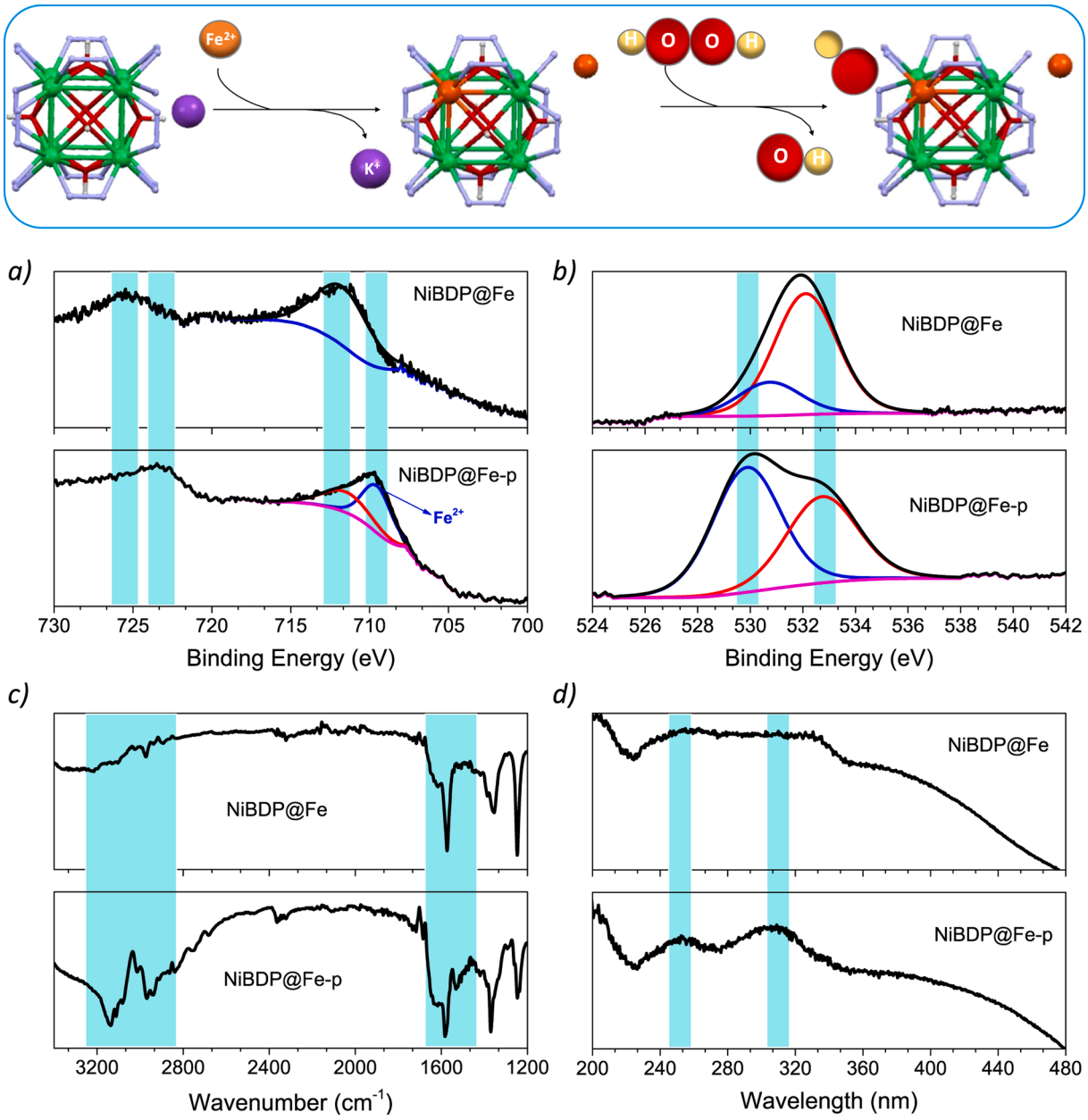

Fig. 1. Top: Schematic representation of the post-synthetic modification of NiBDP@K by ion exchange with $Fe(ClO_4)_2$ to produce NiBDP@Fe and subsequent pretreatment in H_2O_2 to generate NiBDP@Fe-p. For simplicity, only the SBU is shown. Ni (green); K (violet); Fe (orange); N (blue); O (red), H (yellow). Bottom: Iron 2p (a), oxygen 1s (b) XPS signals, FTIR (c) and UV (d) characterization of the Fe(III/II)-OH-like species in NiBDP@Fe before and after the H_2O_2 pretreatment (NiBDP@Fe-p). (For interpretation of the references to colour in this figure legend, the reader is referred to the web version of this article.)

recently reported NiBDP@Fe bimetallic pyrazolate framework obtained from the postsynthetic modification of NiBDP@K (where H_2BDP = 1,4-bis(pyrazol-4-yl), see top part of Fig. 1) [14,15], as Fenton-like catalyst for the activation of H_2O_2 and degradation of p-nitrophenol under mild conditions.

2. Results and discussion

In the first place, the pre- (NiBDP@K) and post-synthetic ion-exchanged MOF (NiBDP@Fe) structure, composition, and stability were determined. The similar XRD patterns for both pre- and post-synthetically iron-doped pyrazolates indicate the preservation of the crystalline structure (see Fig. S1a at the ESI). A slight decrease in porosity upon Fe-exchange (see Fig. S1b at the ESI), mirrored by the decrease of specific surface area from 1380 $m^2 \cdot g^{-1}$ for NiBDP@K to 950 $m^2 \cdot g^{-1}$ for NiBDP@Fe suggests the presence of oxidized $Fe(ClO_4)_3$ occluded in the pores. Thermogravimetric analysis indicates similar thermal stability of both MOFs (see Fig. S1c at the ESI), while the higher amount of volatile components in NiBDP@Fe might be related to the occluded chlorine-containing species combusted during the analysis. According to ICP-OES analysis the Ni:Fe ratio of the final NiBDP@Fe material was 2.7:1, containing minimum amounts of K (Ni:K ratio = 94:1) indicating a successful exchange of the extra-framework potassium ions by iron ions at the NiBDP@Fe.

The oxidation state of iron in the NiBDP@Fe was confirmed by X-ray photoelectron spectroscopy (XPS). The position of the Fe $2p_{1/2}$ and Fe $2p_{3/2}$ bands at 725 and 712 eV, respectively, are ascribed to Fe(III) (refer to Fig. 1a). The iron signal of the H_2O_2 (50 %wt) pretreated material (labeled as NiBDP@Fe-p) shows peaks shifted towards lower BE than the parent one (723.2 *vs* 725.5 eV and 709.7 *vs* 712.2 eV, for the Fe $2p_{1/2}$ and Fe $2p_{3/2}$, respectively). This is probably due to charge donation from the coordinated H_2O_2 and derived ROS to the iron atoms, thus increasing the electron density at metal sites located at the surface. After deconvolution of the Fe $2p_{3/2}$ signal in the H_2O_2 pretreated MOF, one can find evidence of the presence of Fe(II) on the NiBDP@Fe due to a Fenton type reaction (see Scheme 1), as described for other Fe(III) MOFs [11–13]. The oxygen signal of the XPS in the pretreated material has new shoulders at 530.0 eV and 532.8 eV (refer to Fig. 1b), which are shifted ca. 1 eV with respect to the deconvoluted signal of the O 1s peak from the as-prepared MOF (530.7 and 532.1 eV). The broader shoulder at a higher binding energy of 532.8 eV has been attributed to surface peroxide groups (—O_2^{2-}) or absorbed H_2O_2 on the MOF surface [16].

FTIR further confirms a significant absorption at ca. 3100–3200 cm^{-1} in the case of the H_2O_2 pretreated NiBDP@Fe-p sample (see Fig. 1c), suggesting the presence of —OH terminated reactive oxygen species, most likely Fe—OH/OH_2 from the decomposed H_2O_2, as reported previously in the literature [17]. The appearance of new shoulders at 1680, 1630 and 1530 cm^{-1} can be ascribed to the formation of loosely coordinated iron (super)oxide species within the material upon oxidation with H_2O_2. Moreover, the presence of such iron-hydroxyl species upon H_2O_2 peroxide decomposition in the NiBDP@Fe SBUs is also observed at the UV–Vis spectra (Fig. 1d). Two characteristic absorption peaks were observed at around 250 and 310 nm, which have been assigned to absorption induced by ligand-to-metal charge transfer from O(II) to Fe(III) [18], further confirming the XPS shifts toward lower BEs of the iron signals. In addition to the band at ca. 250 nm (probably attributed to Fe^{3+}), a new band around 310 nm appears in the iron MOF after the H_2O_2 treatment, which has been assigned to hydroxylated iron species, e.g. $Fe(OH)^{2+}$ and $Fe(OH)_2^+$, further confirming the formation of hydroxyl anions/radicals at the iron sites [19].

After preparing and characterizing the NiBDP@Fe and NiBDP@Fe-p, their chemical reactivity toward p-nitrophenol (abbreviated here as PNP) at room temperature in an aqueous solution of H_2O_2 was investigated. Given the acidic nature of the phenol group present in PNP (pKa = 7), a slight increase in the pH will lead to the deprotonation of PNP (with maximum absorption at 318 nm) into the corresponding p-nitrophenolate anion, named here as PNPT (with maximum absorption at 400 nm) [20]. In our hands, PNP deprotonation was faster in the presence of the NiBDP@Fe MOF, since the absorbance of PNP decreases 50 % in the presence of the MOF concerning the 40 % decrease in the absence of the MOF (refer to Fig. S3 in the ESI). Although the MOF promotes the generation of hydroxyl-related species, the density of ROS at neutral/basic pH is not sufficient for the oxidation of PNP. Both decreasing the pH (see Fig. 2a) and increasing threefold the concentration of H_2O_2 (see Fig. 2b) favors the degradation of PNP.

Decreasing the pH from ca. 7 to ca. 4, diminishes the protonated PNP absorption by 26 % and the deprotonated PNPT by 77 % (see Fig. 2a). This could be attributed to both the slower H_2O_2 decomposition into H_2O and O_2, as well as the higher density of ·OH produced under acid conditions. Therefore, the increase in the $[H_2O_2]$ goes in line with that of [˙OH] and the amount of PNP that is degraded by such ROS (see Fig. 2b). The best results are obtained for the increase of $[H_2O_2]$ = 353 mM and pH decrease to 4. Under such conditions, PNP is quantitatively oxidized after a few minutes of reaction in contrast to longer times required with carboxylate-based Fe-MOFs [12].

Given the key role of the H_2O_2 pretreatment of the parent MOF in the generation of Fe-OH species and Fe(II) Fenton active sites, we have compared the performance of the parent NiBDP@Fe MOF with the pretreated one (NiBDP@Fe-p) in the degradation of PNP at pH = 4 and $[H_2O_2]$ = 176 mM and using 2 mg of catalyst (see Fig. S4 and Table S1). We have not employed higher MOF and/or H_2O_2 concentrations to avoid complete oxidation which will prevent us from fairly accounting for the H_2O_2 pretreatment effect on the activity. Indeed, the pretreated NiBDP@Fe-p can oxidize 62 % of the PNP in the aqueous sample at 30 °C (see Table S1 and calibration lines for PNP and PNPT in Fig. S12). In contrast, only 42 % of PNP is converted under similar reaction conditions using NiBDP@Fe. The better performance of NiBDP@Fe-p is attributed to the presence of a higher proportion of Fe(II)/Fe(III) at the beginning of the reaction, in contrast to the required (and slower) H_2O_2 promoted Fe(III) reduction (Fenton reaction step). Indeed, a control experiment using the homogeneous Fe(II) or Fe(III) perchlorate precursor indicates the higher activity of the +2 iron sites due to the disappearance of the PNP band (see Fig. S5a). A summary of the physicochemical properties of the MOF and catalytic performance can be found in Table 1.

Finally, we have compared the performance of the MOF before (NiBDP@K-p) and after (NiBDP@Fe-p) the iron exchange, both of them pretreated with H_2O_2 prior to the contact with the aqueous solution of PNP. Under the optimal reaction conditions (pH = 4, 30 °C, 353 mM H_2O_2, and 5 mg of catalyst) the conversion of p-nitrophenol is complete after 5 min in the presence of the NiBDP@Fe-p (refer to Fig. S6). In contrast, the PNP absorbance at its maximum wavelength decreases only 20 % and 14 % (corresponding to its conversion value) in the case of NiBDP@K-p and the blank reaction (in the absence of any MOF), respectively. The low catalytic PNP oxidation activity of NiBDP@K-p with respect to the NiBDP@Fe-p is due to the rapid H_2O_2 decomposition into dioxygen gas and water at the Ni(II) sites [14], instead of the desired aqueous H_2O_2 activation into ROS at the Fe(II)/Fe(III) sites. To support the generation of ROS at the NiBDP@Fe-p we have carried out the PNP oxidation in the presence of one equivalent of p-benzoquinone as a radical scavenger, which quenched the ROS formed, resulting in no PNP degradation (see Fig. S5b).

The phenol degradation rate with the nickel/iron azolate (100 % conversion after 5 min) is higher than that reported for iron-carboxylate MOFs, i.e. MIL-88B-Fe, (100 % conversion after 30 min) under similar reaction conditions (20 °C, pH = 4) and iron:phenol ratio [12]. Moreover, the HPLC analysis of the reaction mixture is shown in Fig. S7. While the PNP peak at a retention time of 15.6 min still appears in the case of using NiBDP@K, this peak is absent when performing the reaction with NiBDP@Fe. To check the resistance of the metal–organic framework under the reaction conditions, we performed the XRD of the recovered material (see Fig. 3). Both the fresh and spent materials

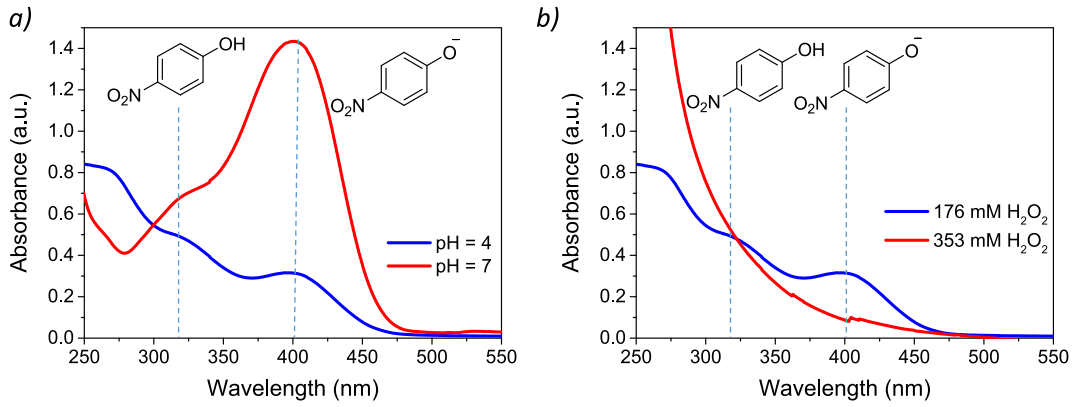

Fig. 2. Oxidation of 1 mL of an aqueous solution of p-nitrophenol (0.3 mM) at 30 °C and different pHs with constant [H_2O_2] = 176 mM (a) or at pH 4 and different [H_2O_2] (b) in the presence of 5 mg of NiBDP@Fe.

Table 1
Catalytic performance of NiBDP@Fe in the PNP (0.3 mM) degradation at pH = 4 and 30 °C.

Sample	Metal composition	Reaction conditions	PNP degraded/ %
Blank	–	353 mM H_2O_2, 60 min	14
NiBDP@K-p	Ni(II)/K(I)	353 mM H_2O_2, 5 mg MOF, 60 min	20
NiBDP@Fe	Fe(III)/Ni(II)	176 mM H_2O_2, 2 mg MOF, 15 min	42
NiBDP@Fe-p	Fe(III)/Fe(II)/Ni (II)	176 mM H_2O_2, 2 mg MOF, 15 min	64
NiBDP@Fe-p	Fe(III)/ Fe(II)/Ni (II)	353 mM H_2O_2, 5 mg MOF, 60 min	>99[a]

[a] After three recycles.

exhibit similar patterns for NiBDP@Fe-p and NiBDP@K-p materials,

indicating the adequate stability of the MOF under the reaction conditions. However, the specific surface area decreases from 950 $m^2 \cdot g^{-1}$ for NiBDP@Fe to 250 $m^2 \cdot g^{-1}$ for NiBDP@Fe-p (see Fig. S8). Moreover, the best-performant NiBDP@Fe-p was recovered and reused three times without apparent iron leaching (according to ICP) and no decrease in PNP conversion after 1 h (Fig. S9).

Given the experimental results and literature precedents [11–14], we propose a tentative mechanism based, first on the coordination of H_2O_2 with Lewis base character to the Fe(III) Lewis acid sites present in the MOF and the subsequent electro-donation between H_2O_2 and the MOF:

NiBDP-Fe(III) + H_2O_2 → NiBDP-Fe(III)-H_2O_2.

This has been corroborated by the Fe-OH signals shown in the FTIR and UV, as well as the Fe 2p and O 1s XPS shifts of the NiBDP@Fe-p with respect to NiBDP@Fe, indicating the partial reduction of some Fe(III) to Fe(II) as indicated in the $Fe2p_{3/2}$ signal of the H_2O_2 pretreated MOF:

NiBDP-Fe(III)-H_2O_2 → NiBDP-Fe(II) + $HO_2^{\bullet}$ + H^+.

Finally, the generated HO· species at the surface of the MOF, or bulk solution will react with PNP, eventually oxidizing it to CO_2 and water (see right part of Scheme 1), as observed by the disappearance of the UV–Vis bands at 318 and 400 nm (see Figs. S2–S6), as well as the HPLC peak of the PNP substrate (see Fig. S7). The recovery of the Fe(III) sites by oxidation with H_2O_2 can be proposed as:

NiBDP-Fe(II) + H_2O_2 → NiBDP-Fe(III) + $HO^{\bullet}$ + OH^-.

3. Conclusions

The combination of iron-doped MOFs with hydrogen peroxide can rapidly remove pollutants (such as p-nitrophenol) from weak acidic room-temperature aqueous conditions. The catalyst design consists of a post-synthetic iron exchange of some of the Ni ions at the framework, together with an H_2O_2 pre-treatment of the sample to increase the Fe (II)/Fe(III) proportion and initiate the Fenton reaction between Fe(II) and H_2O_2. The resulting NiBDP@Fe-p material presents active Fe(II) sites, as well as hydroxyl anions and radicals at the MOF SBUs, according to the spectroscopic characterization of either the sample or the reaction mixture. The MOF maintains its crystalline structure and activity after

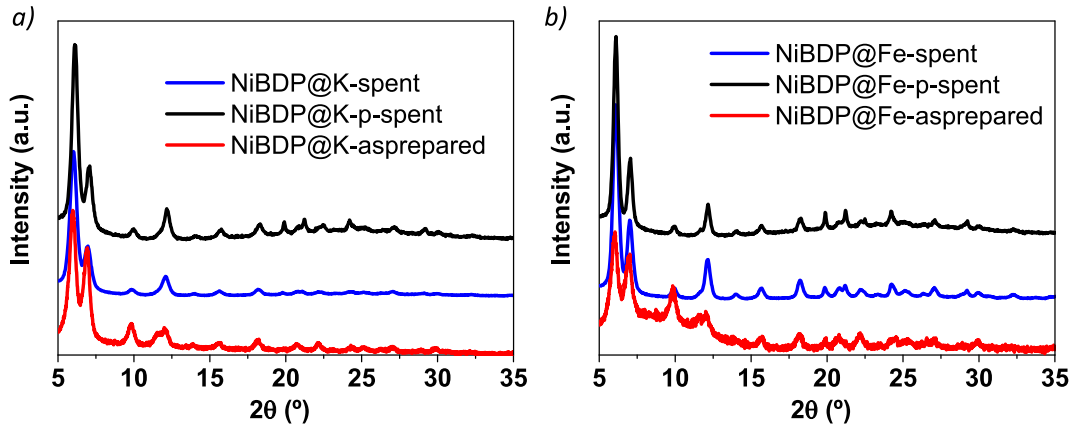

Fig. 3. XRD patterns before (red line) and after reaction for both H_2O_2 pretreated (black line) and non-pretreated (blue line) NiBDP@K (a) and NiBDP@Fe (b) materials. (For interpretation of the references to colour in this figure legend, the reader is referred to the web version of this article.)

several reaction cycles, behaving as a heterogeneous catalyst for the Fenton reaction and p-nitrophenol oxidation. This design and unraveling of active sites as well as the proposal of a reaction mechanism will surely pave the way to other advanced oxidation processes for sustainable pollutant abatement, synthesis of value-added products, and energy-related compounds.

CRediT authorship contribution statement

Nuria Martín: Writing – review & editing, Writing – original draft, Supervision, Investigation, Funding acquisition, Formal analysis, Conceptualization. **Elena López-Maya:** Writing – review & editing, Methodology, Investigation, Formal analysis, Data curation, Conceptualization. **Miguel Maireles-Porcar:** Methodology, Investigation. **Mayra G. Álvarez:** Writing – review & editing, Formal analysis. **Jordi Llorca:** Writing – review & editing, Investigation. **Belén Altava:** Supervision, Funding acquisition. **Eduardo García-Verdugo:** Writing – review & editing, Investigation, Funding acquisition, Formal analysis, Conceptualization. **Francisco G. Cirujano:** Writing – review & editing, Writing – original draft, Supervision, Resources, Project administration, Methodology, Investigation, Funding acquisition, Formal analysis, Data curation, Conceptualization.

Declaration of competing interest

The authors declare that they have no known competing financial interests or personal relationships that could have appeared to influence the work reported in this paper.

Data availability

No data was used for the research described in the article.

Acknowledgments

F. G: C. and N. M. acknowledge the "Ramon y Cajal" contract with code RYC2020-028681-I and RYC2021-033167-I funded MCIN/AEI/10.13039/501100011033 and by "ESF investing in your future", "European Union NextGenerationEU/PRTR". This work has been partially supported by the projects PID2021- 124695OB-C22, PID2022-142897OA-I00 funded by MICINN-FEDER-AEI 10.13039/501100011033, MICIU/AEI/10.13039/501100011033 and by FEDER, UE. The work is also partially supported by the projects TED2021-129626B-I00 and TED2021-130288B-I00/ funded by MCIN/AEI/10.13039/501100011033/ and by the European Union Next Generation EU-PRTR. FGC thank Generalitat Valenciana (CISEJI/2023/78). E. L. M. and M. G. A. acknowledge the research program of University of Salamanca (PIC2-2022-08). J.L. is a Serra Húnter Fellow and is grateful to the ICREA Academia program and projects MICINN/FEDER PID2021-124572OB-C31//AEI/10.13039/501100011033/FEDER, UE and 2021 SGR 01061.

Appendix A. Supplementary material

Supplementary material to this article can be found online at https://doi.org/10.1016/j.inoche.2024.112671.

References

[1] Z.I. Bhatti, H. Toda, K. Furukawa, Water Res. 36 (2002) 1135–1142.
[2] Z. Xiong, H. Zhang, W. Zhang, B. Lai, G. Yao, Chem. Eng. J. 359 (2019) 13–31.
[3] K. Anwar, M. Said, A.F. Ismail, Z.A. Karim, M.S. Abdullah, A. Hafeez, Process Saf. Environ. Protect. 151 (2021) 257–289.
[4] M. Hartmann, S. Kullmann, H. Keller, J. Mater. Chem. 20 (2010) 9002–9017.
[5] A. Ghosh, D.A. Mitchell, A. Chanda, A.D. Ryabov, D.L. Popescu, E.C. Upham, G. J. Collins, T.J. Collins, J. Am. Chem. Soc. 130 (2008) 15116–15126.
[6] R.-S. Yao, M. Sun, C.-L. Wang, S.-S. Deng, Water Res. 40 (2006) 3091–3098.
[7] (a) M. Hartmann, S. Kullmann, H. Keller, J. Mater. Chem. 20 (2010) 9002–9017; (b) H. Ge, M. Cheng, D.L. Huang, M. Yan, Z. Wei, G. Zhang, L. Du, G. Wang, H. Liu, S. Liu, Y. Chen, Chem. Eng. J. 478 (2023) 147369; (c) Q. Shi, N.A. Al-Dhabi, M. Cheng, Y. Liu, J. Wang, G. Wang, G. Zhang, L. Li, L. Du, H. Liu, S. Yang, W. Tang, J. Environ. Chem. Eng. 12 (2024) 112537; (c) C. Tang, M. Cheng, C. Lai, L. Li, Z. Wei, D. Ma, L. Du, G. Wang, L. Yang, L. Tang, J. Environ. Chem. Eng. 11 (5) (2023) 110395.
[8] K. Fajerwerg, H. Debellefontaine, Appl. Catal. B 10 (1996) L229–L235.
[9] A. Bavykina, N. Kolobov, I.S. Khan, J.A. Bau, A. Ramirez, J. Gascon, Chem. Rev. 120 (2020) 8468–8535.
[10] V. Pascanu, G. González Miera, A. Ken Inge, B. Martín-Matute, J. Am. Chem. Soc. 141 (2019) 7223–7234.
[11] S. Lu, L. Liu, H. Demissie, G. An, D. Wang, Environ. Int. 146 (2021) 106273.
[12] C. Gao, S. Chen, X. Quan, H. Yu, Y. Zhang, J. Catal. 356 (2017) 125–132.
[13] J. Joseph, S. Iftekhar, V. Srivastava, Z. Fallah, E.N. Zare, M. Sillanpa, Chemosphere 284 (2021) 131171.
[14] N. Martín, F.G. Cirujano, E. García-Verdugo, J. Llorca, E. Del Río, I. Jiménez-Morales, A. Bogeat-Barroso, E. López-Maya, M.G. Álvarez, ChemPlusChem 12 (2023) e202300447.
[15] E. Lopez-Maya, C. Montoro, V. Colombo, E. Barea, J.A.R. Navarro, Adv. Funct. Mater. 24 (2014) 6130–6135.
[16] H. Li, J. Shang, Z. Yang, W. Shen, Z. Ai, L. Zhang, Environ. Sci. Technol. 51 (2017) 5685–5694.
[17] O. Abuzalat, W.A. El-Mehalmey, H. Tantawy, A. Baraka, Mohamed H. Alkordi, Mater. Adv. 3 (2022) 4262–4267.
[18] L. Ai, C. Zhang, L. Li, J. Jiang, Appl. Catal. B 148–149 (2014) 191–200.
[19] C.C.A. Loures, M.A.K. Alcântara, H.J.I. Filho, A.C.S.C. Teixeira, F.T. Silva, T.C. B. Paiva, G.R.L. Samanamud, Int. Rev. Chem. Eng. 5 (2) (2013). ISSN 2035-1755.
[20] H. Carlos, R. Martínez, C. Dardonville, ACS Med. Chem. Lett. 4 (2013) 142–145.